Long-term aerosol optical hygroscopicity study at the ACTRIS SIRTA observatory: synergy between ceilometer and in situ measurements

Andrés Esteban Bedoya-Velásquez[1,2,3], Gloria Titos[1,2,4], Juan Antonio Bravo-Aranda[1,2], Martial Haeffelin[5], Olivier Favez[6], Jean-Eudes Petit[7], Juan Andrés Casquero-Vera[1,2], Francisco José Olmo-Reyes[1,2], Elena Montilla-Rosero[8], Carlos D. Hoyos[9,10], Lucas Alados-Arboledas[1,2] and Juan Luis Guerrero- Rascado[1,2]

[1]Andalusian Institute for Earth System Research (IISTA-CEAMA), University of Granada, Autonomous Government of Andalusia. Granada, Spain.
[2]Departament of Applied Physics, University of Granada. Granada, Spain.
[3]Sciences Faculty, Department of Physics, Universidad Nacional de Colombia. Medellín, Colombia.
[4]Institute of Environmental Assessment and Water Research (IDAEA), CSIC, Barcelona, Spain.
[5]Institut Pierre Simon Laplace, École Polytechnique, CNRS, Université Paris-Saclay, Palaiseau, France
[6]Institut National de l'Environnement Industriel et des Risques, France
[7]Laboratoire du Climat et des Sciences de l'Environnement (LSCE), France
[8]Physical Sciences Department, School of Science, EAFIT University, Medellín, Colombia.
[9]Facultad de Minas, Departamento de Geociencias y Medio Ambiente, Universidad Nacional de Colombia. Medellín, Colombia.
[10]Sistema de Alerta Temprana de Medellín y el Valle de Aburrá (SIATA), Área Metropolitana del Valle de Aburrá (AMVA)

Correspondence to: Andrés Esteban Bedoya Velásquez (aebedoyav@correo.ugr.es)

Abstract

An experimental setup to study aerosol hygroscopicity is proposed based on the temporal evolution of attenuated backscatter coefficients from a ceilometer colocated with an instrumented tower equipped with meteorological sensors at different heights. This setup is used to analyze a 4.5-year database at the ACTRIS SIRTA observatory in Palaiseau (Paris, France, 2.208 ºE, 48.713 º N, 160 m above sea level). A strict criterion-based procedure has been established to identify hygroscopic growth cases using ancillary information, such as on-line chemical composition, resulting in eight hygroscopic growth cases from a total of 107 potential cases. For these eight cases, hygroscopic growth-related properties, such as the attenuated backscatter enhancement factor $f_\beta\,(RH)$ and the hygroscopic growth coefficient γ, are evaluated. This study evidences that the hygroscopicity parameter γ is negatively correlated with the aerosol organic mass fraction but shows a positive correlation with the aerosol inorganic mass fraction. Among inorganic species, nitrate exhibited the highest correlation.

This is the first time that hygroscopic enhancement factors are directly retrieved under ambient aerosols using remote-sensing techniques, which are combined with on-line chemical composition in situ measurements, to evaluate the role of the different aerosol species on aerosol hygroscopicity.

KEYWORDS: ACTRIS, aerosol hygroscopic growth, hygroscopicity, ceilometer, instrumented tower, remote sensing.

1 Introduction

The role of natural and anthropogenic aerosol particles and greenhouse gases in the climate system has been deeply studied to evaluate the radiative forcing effect on the Earth's surface temperature (Twomey, 1977; Albrecht, 1989). The two major processes of aerosol interactions include (i) the aerosol-radiation interaction (ARI), which produces a direct effect on the Earth's radiative fluxes mainly by scattering and absorbing radiation, and (ii) the aerosol-cloud interaction (ACI) associated with changes in cloud properties and precipitation given that particles can act as cloud condensation nuclei (CCN) and ice nuclei (IN) (Boucher et al., 2013). Both interactions result in a net radiative effect on the global energy budget.

A key factor associated with aerosol radiative forcing is the so-called aerosol hygroscopicity, which is the capacity of particles to uptake water from the environment, changing both the size and chemical composition and thereby influencing the optical properties of aerosols. The magnitude of scattering enhancement depends on the aerosol chemical composition and size, and can be quantified by the hygroscopic enhancement factor $f_{\xi}^{\lambda}(RH)$ where ξ refers to an optical/microphysical property (i.e., backscatter coefficient) and λ is the wavelength. This factor is defined as the ratio between the optical/microphysical property under certain RH conditions and the optical/microphysical property at dry conditions within the volume of atmosphere selected. These studies have been performed using in situ setups, such as humidrograph tandem nephelometers and Humidified Tandem Differential Mobility Analyzer (HTDMA) among others (e.g., Hänel, 1976; Zieger et al., 2011; Titos et al., 2016) as well as remote-sensing instrumentation (e.g., Pilinis et al., 1995; Ferrare et al. 1998; Feingold et al., 2003; Veselovskii et al., 2009; Granados-Muñoz et al., 2015; Bedoya-Velásquez et al., 2018 and references therein). Regarding the in situ setups, there are studies such as Titos et al. (2014a), Zhang et al. (2015) and Zieger et al. (2014), which deeply evaluates the hygroscopic growth properties and their relationship with organic and inorganic chemical composition, evidencing a decreasing tendency between f (RH) and organic aerosols (OA), and an increasing tendency between f (RH) and inorganic aerosols (IA), allowing to evaluate the role of organic and inorganic aerosol on hygroscopic growth studies. These results can be used in global climate models to better constrain aerosol hygroscopic properties with the local and regional emissions. Finally, fewer studies have been performed by crossing information between remote sensing and in situ setups. In Lv et al., (2017) these synergies present interesting approaches for comparing chemical concentrations with hygroscopic growth properties mainly retrieved from lidar

and radiosondes vertical cases studied and good results have been also obtained in Rosati et al. (2016) by comparing airborne in situ with remote sensing on f (RH) calculation.

One of the most used in situ variables for quantifying the diameter increase due to water uptake is the hygroscopic growth factor g (RH) measured with a HTDMA (e.g., Swietlicki et al., 2008). Other instrumentation is used to directly determine the impact of water uptake on aerosol optical properties, such as humidrograph tandem nephelometers that measure the change in scattering coefficient with RH from dry (20-40 %) to wet conditions (up to 90 %) (e.g., Covert et al., 1972; Titos et al., 2016). To quantify the enhancement factor in airborne platforms, instruments, such as the Differential Aerosol Sizing and Hygroscopicity Spectrometer Probe (DASH-SP) (Sorooshian et al., 2008) or the white-light humidified optical particle spectrometer (WHOPS) (Rosati et al., 2015), have been used. A drawback of in situ techniques is the eventual modification of the aerosol properties due to the sampling of atmospheric aliquots by drying and wetting the air sample. Remote-sensing techniques are able to overcome this limitation since they examine particles directly in the atmosphere without any modification of the air sample. Previous remote-sensing studies have combined lidars and radiosondes measurements (e.g., Ferrare et al., 1998; Granados-Muñoz et al., 2015; Fernández et al., 2015) and Raman lidars and microwave radiometers (MWRs) data (Navas-Guzmán et al., 2014, Bedoya-Velásquez et al., 2018) to investigate aerosol hygroscopic growth. Despite their promising capabilities, most of the lidar systems do not operate continuously due to the cost and maintenance requirements; thus, the number of hygroscopic growth cases explored is typically small (Vesolovskii et al., 2009; Granados-Muñoz et al., 2015; Fernández et al., 2018; Bedoya-Velásquez et al., 2018). Unlike sophisticated lidars, automatic lidars and ceilometers (ALCs) are robust systems designed for 24/7 automatic operations. In particular, Vaisala ceilometers have a reduced overlap height with respect to lidars, overcoming the near field of view limitation (Kotthauss et al., 2016).

Haeffelin et al. (2016) demonstrated that an experimental setup combining ceilometer and meteorological measurements from an instrumented tower could be used to forecast fog events, detecting the hygroscopic growth that precedes fog formation. This experimental setup together with ground-based aerosol in situ measurements is used in this study to optimize the selection of hygroscopic growth cases. This methodology is applied to a 4.5-year database of continuous measurements performed at the ACTRIS SIRTA observatory in southern Paris (France). The relationship between the attenuated backscatter β^{att} enhancement factor and submicron aerosol chemical composition is also investigated.

2 Measurement site and instrumentation

2.1 Measurement site

Measurements used in this study were performed at the SIRTA observatory (Site Instrumental de Recherche par Télédétection Atmosphérique, htttp//sirta.ipsl.fr) located approximately 20 km Southwest of Paris city center on the Saclay plateau (2.208 ºE, 48.713 º N, 160 m a.s.l.). This 'supersite' is surrounded by suburban facilities, forests, agricultural fields and roads connecting to Paris. It is part of the European Research Infrastructure for the observation of Aerosol, Clouds, and Trace gases

(ACTRIS) and EARLINET (Pappalardo et al., 2014), including active and passive remote sensing instrumentation operating since 2002 (Haeffelin et al., 2005) and in situ equipment operating continuously since 2011 (Petit et al., 2015). Atmospheric composition measurements performed at SIRTA are considered to be representative of background conditions for the Paris region. Regarding seasonal features, winter and early spring periods frequently experience pollution episodes mainly related to wood-burning, mobile sources (road transportation), and agricultural emissions at a regional scale along with the transport of polluted air masses are associated with high-pressure mesoscale systems (Petit et al., 2014; Petit et al., 2015; Dupont et al., 2016). During summer and autumn, the region remains clean; nevertheless, a maximum impact of road traffic emissions on air quality is noted during the September-October period (Petit et al., 2015).

2.2 Meteorological and in situ aerosol measurements

The meteorological instruments used in this study are located on an instrumented-tower at 1, 2, 5, 10, 20, and 30 m a.g.l. (zone 4, http://sirta.ipsl.fr/documents/ressources/SIRTA_reglementinterieur_2016_Annexe3.pdf, see Fig. 1) described in Haeffelin et al. (2016). Here, we use meteorological measurements at 30 m a.g.l. and ceilometer (Vaisala CL31) measurements. Temperature and relative humidity were obtained from Young 41382 and 43408 sensors with a temporal resolution of 1 min. Wind velocity and direction were measured using a sonic anemometer (Metec sonic anemometers) operating at 10 Hz for raw data (1 min-averaged) with uncertainties of 0.1 m/s and ± 2° for speed and direction, respectively.

Aerosol chemical composition of non-refractory submicron aerosols was obtained with an Aerosol Chemical Speciation Monitor (ACSM, Aerodyne Research, Inc.). A detailed description of measurement principles of this instrument can be found in Ng et al. (2011). Briefly, it notably allows measurements of concentrations of major submicron chemical species, including organic aerosol (OA), ammonium (NH_4^+), nitrate (NO_3^-) and sulfate (SO_4^{2-}), particles, with a temporal resolution of 30 min using online thermal desorption electron impact aerosol mass spectrometry. Black carbon (BC) mass concentration was obtained from measurements of the absorption coefficient at 880 nm performed with a multiwavelength Aethalometer (AE33 model, Magee Scientific) at 1-min resolution. The AE33 measurement principle is described in Drinovec et al. (2015). In the present study, concentrations of BC and non-refractory chemical species are used as hourly data, and PM_1 mass concentration is estimated as the sum of these compounds. Both ACSM and AE33 measurements are subject to ACTRIS (http://www.actris.eu) quality control and quality assurance procedures, notably participating in regular intercomparison exercises at the European Center for Aerosol Calibration (e.g., https://www.actris-ecac.eu/files/ECAC-report-AP-2017-4-2.pdf; Crenn et al., 2013; Freney et al., 2016). A full description of the calibration and data treatment methods for both AE33 and ACSM used in the present study are presented by Petit et al. (2017) and Petit et al. (2015), respectively. The in situ monitoring station is located 5 km east of the instrumented tower (SIRTA zone 5, Fig. 1b).

2.3. Vaisala CL31 ceilometer

A Vaisala CL31 ceilometer colocated with an instrumented-tower is used in this study. Ceilometers have two principal advantages compared with more powerful lidar systems typically used for atmospheric research. Ceilometers can reach their full overlap height between 20–200 m and allow unattended 24/7 operation. CL31 ceilometers operate using the lidar's principle by emitting radiation towards the atmosphere at 910 nm on a mono-axial configuration with a repetition rate of 10 kHz and high-spatial and -temporal resolution (15 m and 30 s, respectively). The total backscattered signal $P\ (z,t)$ from the CL31, accounting for both the aerosol and molecular signature, is defined as follows:

$$P(z,t) = \frac{1}{z^2}\ \mathrm{C}\ (\mathrm{t}) O(z,t)\beta(z,t)\ T^2(z,t) T_{wv}^2(z,t) \tag{1}$$

where z is the signal range, t is the time, $O(z,t)$ is the overlap function, C (t) is the calibration constant, $\beta(z,t)$ is the total backscatter coefficient due to particles and molecules, $T(z,t)$ is the attenuation due to particles and molecules, and $T_{wv}(z,t)$ is the attenuation due to water vapor molecular absorption of the laser light at 910 nm (Wiegner et al. 2015). Both transmittances are defined as follows:

$$T(z_1, z_2, t) = exp\left(-\int_{z_1}^{z_2} \alpha_T(z,t)dz\right) \tag{2}$$

$$T_{wv}(z_1, z_2, t) = exp\left(-\int_{z_1}^{z_2} \sigma_{a,wv}(z,t)dz\right) \tag{3}$$

where α_T is the total extinction coefficient, including the extinction due to particles (α_{par}) and molecules (α_{mol}); $\sigma_{a,wv}$ is the water vapor absorption coefficient in the atmosphere, and z_1 and z_2 define the region where the air volume of interest is located.

The attenuated backscatter is typically defined by the backscatter attenuated by particles and molecules as follows:

$$\beta^{att}(z,t) = \beta(z,t)\ T^2(z,t) \tag{4}$$

Due to the wavelength of operation, the CL31 signal also includes the water vapor absorption resulting as follows:

$$\beta_{wv}^{att}(z,t) = \beta^{att}(z,t) T_{wv}^2(z,t) = \frac{P(z,t)z^2}{\mathrm{C}\ (\mathrm{t}) O(z,t)} \tag{5}$$

The CL31 signal is affected by different aspects, such as external temperature variations and the geometry of the emission and reception systems (mainly linked with overlap) among others (Madonna et al., 2015). We assume the errors reported for β^{att}coefficients are up to 10 % or less following that reported by Wiegner and Geiβ (2012).

3. Methodology

3.1 Experimental setup

Most of the studies investigating the effect of aerosol hygroscopicity in aerosol optical properties have focused on the particle scattering coefficient (σ_{sp}) measured with in situ techniques (e.g., Covert et al., 1972; Sorooshian et al., 2008; Zieger et al., 2011; Titos et al., 2016). More recently, remote sensing measurements have been used to investigate aerosol hygroscopicity using the particle extinction coefficient (Veselovskii, et al., 2009) and particle backscattering coefficient (Granados-Muñoz, et al., 2015, Fernández et al., 2018, Bedoya-Velásquez et al., 2018). These studies use the enhancement factor $f_\xi\,(RH)$ defined as follows:

$$f_\xi(RH) = \frac{\xi(RH)}{\xi(RH_{ref})} \tag{6}$$

where ξ represents an aerosol optical/microphysical property evaluated at certain RH. RH_{ref} refers to a reference (dry) condition. The most common parameterization linking $f_\xi\,(RH)$ with RH was proposed by Hänel et al. (1976):

$$f_\xi(RH) = \left(\frac{1-RH/100}{1-RH_{ref}/100}\right)^{-\gamma}, \tag{7}$$

where γ parametrizes the aerosol hygroscopic enhancement (larger values of γ are related to more hygroscopic aerosol particles).

To investigate aerosol hygroscopicity, we use the experimental setup proposed by Haeffelin et al. (2016) (Figure 1) consisting of a Vaisala CL31 ceilometer colocated with a meteorological instrumented-tower. This setup allows for simultaneous tracking of the β_{wv}^{att} and RH changes at 30 m a.g.l. (z_{ref}). Thus, the attenuated-backscatter enhancement factor affected by absorption of water vapor $f_{\beta_{wv}^{att}}(RH)$ is expressed as follows:

$$f_{\beta_{wv}^{att}}(RH) = \frac{\beta_{wv}^{att}(z_{ref},t)}{\beta_{wv}^{att}(z_{ref},t_d)} = \frac{\beta^{att}(z_{ref},t)T_{wv}^2(z_{ref},t)}{\beta^{att}(z_{ref},t_d)T_{wv}^2(z_{ref},t_d)}, \tag{8}$$

where t_d refers to the dry state of the aerosols within the temporal window of evaluation. Then, replacing from Eq. (5), the following formula is obtained:

$$f_{\beta_{wv}^{att}}(RH) = \frac{P(z_{ref},t){z_{ref}}^2/\mathrm{C}\,(t)O(z_{ref},t)}{P(z_{ref},t_d){z_{ref}}^2/\mathrm{C}\,(t_d)O(z_{ref},t_d)}. \tag{9}$$

Assuming that the calibration factor and the overlap function are sufficiently stable during the period considered, the attenuated-backscatter enhancement factor affected by absorption of water vapor can be expressed as follows

$$f_{\beta_{wv}^{att}}(RH) = \frac{P(z_{ref},t)}{P(z_{ref},t_d)}, \tag{10}$$

Thus, we can directly retrieve $f_{\beta_{wv}^{att}}(RH)$. Finally, we need to estimate the transmittance ratio due the water vapor absorption to determine $f_{\beta^{att}}$ as follows:

$$f_{\beta^{att}}(RH) = f_{\beta_{wv}^{att}}(RH)\frac{T_{wv}^2(z_{ref},t_d)}{T_{wv}^2(z_{ref},t)}. \quad (11)$$

The water vapor term can be rewritten using Eq. (3):

$$\frac{T_{wv}^2(t_d)}{T_{wv}^2(t)} = exp\left(-\int_{z_1}^{z_2}\left(\sigma_{a,wv}(t_d) - \sigma_{a,wv}(t)\right)dz\right), \quad (12)$$

where the dependence of height has been omitted for the sake of clarity. Following Wiegner et al. (2015), the extinction coefficient due to water vapor absorption is given as follows:

$$\sigma_{a,wv}(t) = n_{wv}(t)\sigma_{wv} = 7.25 \cdot 10^{22}\, q(t) R_{wv}\sigma_{wv}, \quad (13)$$

where σ_{wv} is the water vapor absorption cross-section, and $n_{wv}(t)$ refers to the water vapor concentration. $R_{wv} = 0.462\, Jg^{-1}K^{-1}$ is the gas constant of water vapor, and q is the absolute humidity. For this evaluation, we assume that $\sigma_{wv} = 2.4 \cdot 10^{-22} cm^2$ is simulated at 908.957 nm (Wiegner et al., 2015, 2018). Then, replacing Eq. (13) with Eq. (12), we obtain the following:

$$\frac{T_{wv}^2(t_d)}{T_{wv}^2(t_w)} = \exp\left(-2\int_{z_1}^{z_2}\left(\sigma_{a,wv}(t_d) - \sigma_{a,wv}(t)\right)dz\right) = \exp\left(-2K_{wv}\int_{z_1}^{z_2}(q(t_d) - q(t))dz\right) = \exp(-2K_{wv}\Delta q \Delta z) \quad (14)$$

where K_{wv} gathers all the constants, such as σ_{wv}, R_{wv}, Δz (30 m agl in our instrument setup), and $\Delta q = q(t_d) - q\,(t)$. An important fact shown in Eq. (14) is that water vapor correction is only affected by the relative difference of the absolute humidity in the explored temporal frame. The setup used allows us to obtain the experimental value of $q(t)$ to perform the calculation proposed in Eq. (14).

Once the $f_{\beta^{att}}(RH)$ is obtained, we must address the fact that β^{att} is influenced by the transmittance of the atmospheric layer between the surface and 30 meters. In this regard, the link between the attenuated backscatter coefficient (β^{att}) and particle backscatter coefficient (β) at 30 m was evaluated in detail in Haeffelin et al. (2016) to guarantee the suitability of using the attenuated backscatter for hygroscopicity studies. Indeed, Haeffelin et al. (2016) found that differences between $f_{\beta^{att}}(RH)$ and the particle backscatter enhancement factor $f_{\beta}(RH)$ to be lower than 10 % by assuming a lidar ratio between 30 and 80 sr (at RH_{ref}) in the simulations and $f_{\alpha}\,(RH) > f_{\beta^{att}}\,(RH)$. Therefore, in the manuscript, we will assume hereafter that $f_{\beta^{att}}(RH) \cong f_{\beta}(RH)$; therefore, β^{att} will be treated as β from this point forward.

Additionally, to make this study comparable with most applied in situ approaches, we performed the calculation of $f_\beta(RH)$ using two approaches. The first approach considers the RH_{ref} as the lower value of RH in the atmosphere within the time-window of evaluation, and the second approach takes an extrapolation of the $f_\beta(RH)$ to RH_{ref}= 40 %, assuming such value of RH_{ref} as the driest one in the atmosphere. This second approach becomes important only because this work pretends to be compared with in situ studies. An important fact of this extrapolation is that it uses the same γ parameter; therefore, the same aerosol is studied. The RH_{ref} extrapolated values presented a percentage differences greater than those found in this study, suggesting that theoretically the aerosol should be dry at lower RH than atmosphere shown; however, atmosphere takes into account different processes that surely modifies theoretical extrapolated RH_{ref} found.

3.2. Data preprocessing and uncertainties estimation

To homogenize the different datasets, CL31 measurements were averaged to the same temporal resolution as RH measurements (i.e., 1 min). Then, $f_\beta(RH)$ was determined using Eq. (6) to retrieve γ using Eq. (7). The error associated with γ was calculated using the Monte Carlo technique, modeling raw measurements of β and RH as normal distributions and β_{ref} and RH_{ref} as the respective values calculated for each case and finally assuming the error as the mean standard deviation of all simulations. The uncertainty of $f_\beta(RH)$ was also estimated using the Monte Carlo technique by using the values of γ found and the same modeling previously performed for β and RH. The estimated error of applying the water vapor correction to β^{att} was obtained as the bias between β^{att} and β_{wv}^{att} for the cases studied, which is less than $2.5 \cdot 10^{-7}$ $m^{-1} \cdot sr^{-1}$ (see the supplementary material for further details). The uncertainty of this correction was also calculated using the Monte Carlo technique by applying Eq. 7, modeling β^{att} and T_{wv}^2 as normal distribution and running this procedure 10000 times. With this procedure, we obtained an error of approximately $3.0 \cdot 10^{-7}$ $m^{-1} \cdot sr^{-1}$. It is important to mention that the use of this methodology could lead to larger uncertainties than those reported in previous in situ or collocated lidar hygroscopic studies, which are mostly associated with instrumental error propagation.

3.3. Aerosol hygroscopic optical enhancement identification

The main challenge when dealing with real (i.e., uncontrolled) atmospheric conditions is the ability to isolate the hygroscopic enhancement effect from all other processes that occur simultaneously (changes in air masses, emissions or advected aerosol particles from local sources). Therefore, we designed a methodology to (i) identify potential hygroscopic enhancement events when there is an observed increase in the attenuated backscatter coefficient simultaneously to an increase in ambient RH and to (ii) elucidate whether those increases are due to hygroscopic growth. To evaluate these conditions, we propose four phases in which different instrumentation is involved with the aim of extending its applicability depending on the instrument availability:

Phase 1: Preprocessing of ceilometer data. This step includes the corrections mentioned in section 3.1 as well as the water vapor correction explained in section 3.2. Additionally, the data are averaged in 1-min intervals.

Phase 2: Selection of potential hygroscopic growth cases. Potential cases have been selected by looking for simultaneous increases/decreases in β and ambient RH. To this end, a 3- to 5-hour sliding temporal window has been used. Time windows larger than 5-h are avoided to minimize the influence of changing emission sources and air masses.

Phase 3: Hänel parameterization of potential cases. After applying Hänel parameterization (Eq. 7), we select only those cases that fulfil the following:

i. $R^2 > 0.80$, assuring high data-correlation following Hänel parameterization.
ii. $\Delta RH > 30$ %, where ΔRH refers to the difference between final and initial RH within the temporal window under study. This criteria is used to apply the Hänel parameterization over a sufficient RH-range.
iii. $RH_{ref} < 60$ %, allow us to choose the driest β_{ref} without losing potential hygroscopic growth cases.
iv. The analysis is restricted to RH < 99 % to avoid air masses with RH=100 % or those that are supersaturated.
v. Low variability (< 35 %) in both wind speed and direction. Based on the analysis of wind speed $W_s(t)$ and wind direction $W_d(t)$, this criterion aims to minimize the impact of changing air masses during the time window under evaluation. Numerically, this variability is calculated by dividing the standard deviation by the mean value.

Phase 4: Additional information on aerosol concentration is needed to discard the notion that the increase observed in β is not related to an increase in the aerosol mass concentration but due to an increase in RH. In our case, we used data from the ACSM and Aethalometer given the advantage that we can specifically assess aerosol chemical components. In this step of the methodology, we define the ratio-index (RI) as the ratio between $f_\beta(RH)$ and $f_{PM1}(RH)$, in order to evaluate whether the increase in β is associated with an increase in the aerosol load. Therefore, we rejected those potential hygroscopic enhancement cases that showed RI < 0.5.

After applying the aforementioned methodology to 4.5 years of continuous measurements at the ACTRIS SIRTA observatory (from 01st January 2012 to 19th June 2016), we identified 107 potential cases of aerosol hygroscopicity enhancement (phases 1 and 2). The number of hygroscopic growth cases fulfilling 3.i and 3.ii was reduced to 64 cases. Continuing with the phases proposed here, once we performed the following steps (3.iii, 3.iv, 3.v and phase 4), we obtained 8 cases in which we can assure that the enhancement in the attenuated backscatter coefficient is due to aerosol hygroscopicity. Despite the significant reduction in the number of hygroscopic growth cases from the 107 initial potential cases, the methodology presented here allowed us to disregard those cases in which the enhancement can be attributed to increase in RH or changing aerosol type or load. This is the first time that remote-sensing-derived aerosol hygroscopicity has been investigated in such detail thanks to the availability of colocated in situ measurements. The eight cases identified are analyzed in detail in the following section.

4. Results and discussion

4.1 Two case studies of the methodology implementation

As an example of the methodology implementation, this section shows two of the final eight hygroscopic growth cases found in this study (Fig. 2 and Fig. 3). These examples correspond to 25 June 2013 from 07:17 to 10:17 UTC (case 3) and 17 May 2016 from 07:40 to 10:40 UTC (case 8). Fig. 2a and Fig. 3a present the time evolution of β, T, RH, q, W_s, W_d, dew point temperature T_d, and 1-h averaged aerosol chemical composition (BC, OA, NH_4^+, NO_3^- and SO_4^{2-}). The shadowed region in Fig. 2a and Fig. 3a highlight the selected time-window in which β and RH simultaneously increases/decreases. Figure 2b and Fig. 3b show $f_\beta(RH)$ and $f_{PM1}(RH)$, and Fig. 2c and Fig. 3c contain a pie chart with the mean contribution of each chemical compound during the hygroscopic event. These cases were selected to show two different situations found in this study (the other six cases are shown in Figures S5-S10 of the supplementary material). Once a simultaneous monotonic decrease was observed for β and RH in cases 3 and 8, we apply the Hänel parameterization, obtaining the corresponding γ and f_β $(RH = 85\ \%)$.

Case 3 presents lower value of hygroscopicity parameter, with values of $\gamma = 0.5 \pm 0.4$ and f_β $(RH = 85\ \%) = 1.7 \pm 0.2$. During case 3, the predominant wind direction was NW with relatively low wind speed ($W_s = 2.5$ m/s) and some variability up to ΔW_s =24.5 % and $\Delta W_d = 33.9$ %, and the chemical composition was relatively constant in most compounds over the time window studied. The average chemical composition (Fig. 2c) indicated a high contribution of OA (58 %) and BC (17 %) particles, and the total aerosol mass (PM_1) was almost constant during the hygroscopic case (from 7:17 to 10:17 UTC), showing no correlation with RH. The relative high presence of BC and OA (less hygroscopic compounds) may reduce the hygroscopicity properties. These findings are consistent with results from rural and suburban sites presented by Chen et al. (2014) in Wuqing (China), Zieger et al. (2014) in Melpitz (Germany) and Titos et al. (2014a) in Granada (Spain), where low value of hygroscopicity parameters were observed due to high contribution of OA and BC. A detailed discussion of the origin of the air masses will be given in Sec. 4.2.

Case 8 presents predominant westerly wind with a relatively high mean wind speed (5 m/s) and low variability in both wind speed and wind direction (ΔW_s =20.7 % and $\Delta W_d = 6.4$ %), and a slight increase in PM_1 with RH was observed (Fig. 3b). However, the enhancement of β is significantly higher with respect to the variation in PM_1. In fact, the RI remains within the selected range (RI= 0.60), denoting that most of the increase in the attenuated backscatter coefficient can be attributed to hygroscopic growth. The chemical composition during case 8 shows a predominance of OA (46 %) but also with important contribution of secondary inorganic compounds SO_4^{2-} (19 %) and NH_4^+ (12 %), which are highly hygroscopic, and low contribution of BC (8 %). This case exhibited higher aerosol hygroscopic properties than case 3 with $\gamma = 0.9 \pm 0.6$ and f_β $(RH = 85\ \%) = 2.5 \pm 0.3$. This behavior might be linked to the lower contribution of OA and BC and higher contribution

of inorganic aerosols (IA). Studies performed close to the SIRTA site by Randriamiarisoa et al. (2006) at Saclay (France) report a high $\gamma = 1.04$ and f_σ $(RH = 80\ \%) \sim 2.0$ linked to a low contribution of OA and high IA contribution associated with anthropogenic and marine aerosols. A more in-depth description of this case will be given in the following sections.

4.2 Relationship between aerosol hygroscopicity properties and chemical composition

Table 1 reports the eight aerosol hygroscopic growth cases found with the described methodology presented in section 3.3 applied to the 4.5-year database. In general, most of the air masses (calculated by HYSPLIT model, but not shown here) came from Canada, Greenland and Iceland, passing through the Atlantic Ocean and then crossed United Kingdom before reaching France, therefore suggesting a mixture of marine aerosols with other types such as urban, anthropogenic, among other local sources found in this study. Three cases were observed in spring (case 6, case 7 and case 8), presenting relatively high concentrations of SO_4^{2-} and NO_3^- with the exception of case 8 in which NH_4^+ was higher than NO_3^- (case 6 with 11 % (SO_4^{2-}) and 21 % (NO_3^-,), case 7 with 36 % (SO_4^{2-}) and 10 % (NO_3^-), and case 8 with 19 % (SO_4^{2-}) and 1 % (NO_3^-,) respectively, with high concentration of NH_4^+ (12 %)). The high sulphate concentration in this season could be mainly related to the advection of air masses containing petrochemical and shipping emissions over this area and the typical increases of the nitrate and ammonia in spring that might be linked to the formation of particulate ammonium nitrate from road transport and agricultural gaseous emission under favorable meteorological conditions (Petit et al., 2015). Four cases were found in summer (case 1, case 3, case 4, and case 5), a period of the year commonly characterized by low wind speed at the ACTRIS SIRTA observatory (Petit et al., 2015), which reduces long-range transport of aerosol particles. Finally, a case was observed in September (case 2) showing the highest concentrations of PM_1 up to 10 µg/m^3 with a major presence of OA (56 %), SO_4^{2-} (18 %) and NH_4^+ (15 %). All these cases occurred between 6:00 and 14:00 UTC when the temperature increased monotonically with almost constant absolute humidity; thus, RH decreased. In this area, the OA is considered as a regional background component that dominates the PM_1 chemical composition independent of the wind direction (Petit et al., 2015). According to previous studies, the higher concentrations of OA observed in this region might be associated with local influence, mainly in winter and autumn given the increase in wood-burning and road traffic pollution (e.g., Zhang et al., 2007; Putaud et al., 2010; Petit et al., 2014; Petit et al., 2015).

Cases 2, 4 and 6 present values similar to the values reported by Fernández et al. (2015) of f_β $(RH = 85\ \%) = 2.04$ with $\gamma = 0.589 \pm 0.007$ at Cabauw station (Netherlands) using lidar measurements with the presence of marine salt particles, ammonium nitrate and organic matter. The composition of these particles was linked to anthropogenic activities, oceanic air masses, and agriculture over this region. In addition, Fernández et al. (2018) found values of $f_{\beta^{par}}$ $(RH = 85\ \%) = 2.05$ ($\gamma = 0.92 \pm 0.02$) for marine particles based on measurements from the Madrid-CIEMAT station (Spain) that are close to the values of cases 7 and 8 in our study. These results from the literature are consistent with the predominant chemical composition found

in our study. Case 5 exhibited relatively high concentrations of SO_4^{2-} (20 %) and OA (58 %), leading to f_β ($RH = 85$ %)= 1.6 ± 0.1 ($\gamma = 0.5 \pm 0.2$). These values are comparable with those reported by Bedoya-Velásquez et al. (2018) for a mixture of anthropogenic and smoke particles at the IISTA-CEAMA station (Granada, Spain). Nevertheless, the values presented in this work are not fully comparable with previous remote-sensing literature since the f_β (RH) is derived at 910 nm, whereas most enhancement factor values in the literature are reported at 532 nm. This fact would slightly change the efficiency of the backscatter cross sections of the aerosol particles analyzed; consequently, f ($RH = 85$ %) may also change. Another difference with most remote-sensing studies is that we studied the temporal change of the aerosol hygroscopicity (RH and β), while most studies investigate the vertical change.

The results obtained in this study can also be compared with previous studies based on in situ data, taking into account that the remote-sensing and in situ techniques have different working principles and the intrinsic difference of the optical property investigated (attenuated backscatter coefficient and integrated scattering coefficient). Remote-sensing operates under unmodified ambient conditions, and the optical property evaluated is β. In contrast, hygroscopic growth in situ measurements are performed by controlling RH (starting mostly from RH_{ref}=40 %) and uses σ_{sp} (scattering coefficient) as the optical property. Therefore, the results between techniques are not directly comparable. Thus, to make the studies more comparable, we performed an extrapolation of f_β ($RH = 85$) to 40 % which is the RH_{ref} mostly used in the in situ studies. The cases with lower hygroscopic properties in our study are cases 1, 3 and 5, presenting f_β ($RH = 85/40$ %)$\sim 2.3 \pm 0.2, 2.0 \pm 0.2, 2.0 \pm 0.1$ with γ=0.6$\pm$0.6, γ=0.5$\pm$0.4 and γ=0.5$\pm$0.2, respectively. Similar values are reported for f_σ ($RH = 80/40$ %) and f_σ ($RH = 85/40$ %) at RH_{ref}=40 % by Sheridan et al. (2002) in the Indian Ocean, Titos et al. (2014b) in Cape Cod (US) and Chen et al. (2014) in Wuqing (China) for polluted, marine and mixed aerosols (urban and suburban) using in situ techniques. In this study, these three cases have low NO_3^- concentrations and relative higher OA and BC concentrations, which highlight an aerosol mixture with the predominance of less hygroscopic particles compared with the other five cases. Cases 2, 4, 6, 7 and 8 presented similar values of f_β ($RH = 85/40$ %) ranging from 2.6 to 3.3, while γ lay between $0.7 < \gamma < 0.9$, showing a higher NO_3^- concentration with the exception of case 8 that exhibited higher concentrations of SO_4^{2-} and NH_4^+. The f_β ($RH = 80$ %) and γ values can be well compared to reported ones found in in situ studies performed by Kotchenruther et al. (1999) (East Coast, US) and Randriamiarisoa et al. (2006) (Saclay, France) that probed air masses influenced by anthropogenic and marine (clean and polluted) aerosols.

Table 2 presents the relationship between chemical composition and aerosol hygroscopicity. To this end, we calculated the organic mass fraction (OMF) defined as OA mass concentration divided by the total mass concentration (PM_1) and inorganic mass fraction (IMF) calculated as the IA divided by the total mass concentration. Figure 4a shows an anti-correlation between OMF and γ (y= (-1.5 ± 0.1) x + (1.5 ± 0.1), R^2= 0.67), and Fig. 4b shows that IMF exhibits a positive correlation with γ (y= (1.2 ± 0.1) x + (0.2 ± 0.1), R^2= 0.42). To compare both hygroscopic properties (f ($RH = 85$) and γ) with in situ literature, we

also performed a linearization of the $f\ (RH = 85)$ extrapolated to 40 % using this value as a reference for dry conditions, evidencing the same tendency for OMF (y= (-4.81 ± 0.04) x + (5.3 ± 0.1), R^2= 0.60) and IMF (y= (3.8 ± 0.1) x + (1.1 ± 0.1), R^2= 0.40) but with higher slopes. These results are consistent with in situ studies that correlate the chemical composition with $f_\sigma\ (RH = 85/40)$ and γ, showing that aerosol hygroscopicity decreases as the relative contribution of OA in the total aerosol load increases (e.g., Kamilli et al., 2014; Zieger et al., 2014; Titos et al., 2014a; Zhang et al., 2015; Jefferson et al., 2017 and Chen et al., 2018).

The slopes presented in Table 2 for $f_\beta\ (RH = 85/40\ \%)$ versus OMF and IMF are in good agreement with the results expected according to the literature, showing a negative correlation of $f_\beta\ (RH = 85/40\ \%)$ with OMF and positive correlation with IMF. However, the slopes are substantially higher than those reported by Zieger et al. (2014) at Melpitz (Germany), namely, a slope of OMF with γ of -3.1 ± 0.1 with R^2= 0.57 and a slope of IMF with γ of 2.2 ± 0.1 (R^2=0.57).

Similar tendencies were also reported by Zhang et al. (2015) at Lin'an, China for OMF (slope of -1.20 and R^2= 0.88) and IMF (slope of 0.93 and R^2=0.57). Similarly, Titos et al. (2014a) reported a slope of -1.9 (R^2 = 0.74) at an urban site in Southern Spain. The in situ slope values are significantly lower compared with our results extrapolated to RH_{ref}=40 %. These differences are likely due to the different measurement techniques. Since this is the first remote sensing based hygroscopicity study that includes chemical composition, this comparison is not straightforward. However, a clear tendency exists.

To identify the inorganic compound that plays a stronger role in aerosol hygroscopicity, we performed the calculation of the relative amount of OA ($F_o = C_{OA}/(C_{OA} + C_{IA})$) against γ, where C_{OA} and C_{IA} are the mass concentration of organic and inorganic aerosols, respectively. This calculation showed two different trends when NO_3^- and NH_4^+were added, showing that NO_3^- has a more pronounced negative correlation than NH_4^+. The relative amount is determined by the calculation of $F_o = OA/(OA + SO_4^{2-} + NO_3^-)$ with fitting line y= (-1.2± 0.2) Fo + (1.4± 0.1) R^2=0.40 and $F_o = OA/(OA + SO_4^{2-} + NO_3^- + NH_4^+)$ y= (-1.3± 0.2) Fo + (1.4± 0.1) R^2=0.51. Then, we performed an individual calculation for each inorganic compound, and $F_o = OA/(OA + SO_4^{2-})$ showed the lowest correlation coefficient ($y = (-0.7 \pm 0.2)\ Fo + (1.2 \pm 0.2)$, R^2=0.18), followed by $F_o = OA/(OA + NH_4^+)$ with a slightly high correlation (y=(- 1.1± 0.1) Fo + (1.6± 0.1) R^2=0.26). Then, the correlation increased for $F_o = OA/(OA + NO_3^-)$ (y=(- 1.3± 0.1) Fo + (1.8± 0.1), R^2=0.32), suggesting that $NO_3^-$is more determinant than other inorganic compounds at the ACTRIS SIRTA station as an aerosol hygroscopic compound. The tendencies found can be compared with those obtained in Zhang et al. (2015) at Lin'an, China where NO_3^- played a stronger role than SO_4^{2-}. These findings indicate that increases in NO_3^- are associated with decreases in $SO_4^{2-}$by the Shanghai megacity influence.

5. Conclusions and perspectives

In this work, a new methodology was successfully applied to investigate aerosol hygroscopic growth based on a 4.5-year dataset obtained at the SIRTA observatory in the Paris region (2.208 ºE, 48.713 º N, 160 m a.s.l.). To our knowledge, this is the first time that such a study was conducted under unmodified atmospheric conditions using long-term in situ and ceilometer instrumentation. Among 107 potential cases of hygroscopic growth provided by the proposed procedure, 8 cases were clearly identified as fulfilling the strictly defined criteria to isolate events when the hygroscopic enhancement effect dominated all the other possible atmospheric processes.

The hygroscopic parameters were compared to on-line chemical composition measurements. All cases presented high concentrations of OA, which is considered as a background component over the study region. Hygroscopic growth properties were compared with previous remote-sensing and in situ studies, and similar values for anthropogenic, polluted marine and mixed particles (urban and suburban areas) were obtained.

The relationship between chemical composition and γ parameter was evaluated, revealing that hygroscopicity backscattering enhancements decrease linearly as the contribution of organic aerosols increases. In this sense, the organic mass fraction (OMF) is anticorrelated with γ and f_β ($RH = 85/40$), while IMF shows a positive correlation with γ and f_β ($RH = 85/40$). This relationship of OMF and IMF is consistent with the literature; however, the magnitude of the trend varies among studies. These tendencies indicate that the role of IA is a determinant in the aerosol hygroscopic growth behavior. To determine the inorganic compound role, we calculated the contribution of SO_4^{2-}, NO_3^- and NH_4^+ to the IA concentrations and demonstrated that NO_3^- plays a more important role than other inorganic compounds in hygroscopic growth studies in this region.

As we evaluate the role of IA in aerosol hygroscopicity, it is important to conduct detailed studies on the role of OA given that these components can be soluble. Thus, further research on this topic may focus on the role of the different OA fractions, such as hydrocarbon-like organic, peat and nonpeat biomass burning and oxygenated organic aerosols, in aerosol hygroscopic properties. A relevant aspect is associated with aerosol acidification that should be evaluated to determine the role of aged or fresh aerosols in hygroscopic properties and their impacts on OA. Finally, further investigation extending the study period is important to obtain statistically robust results over this region using automatic remote sensors.

Coauthor contributions

Andrés Esteban Bedoya-Velásquez, Gloria Titos, and Juan Antonio Bravo-Aranda designed and performed the experiments. Gloria Titos ran the code. Andrés Esteban Bedoya-Velásquez and Juan Antonio Bravo-Aranda processed the ceilometer signal.

Olivier Favez and Jean-Eudes Petit prepared the in situ data. Andrés Esteban Bedoya-Velásquez wrote the manuscript with contributions from all coauthors.

Acknowledgements

This work was supported by the Andalusia Regional Government through project P12-RNM-2409; the Spanish Ministry of Economy and Competitiveness through projects CGL2013-45410-R, CGL2016-81092-R and CGL2017-83538-C3-1-R; the Excelence network CGL2017-90884-REDT; the Juan de la Cierva grant IJCI-2016-29838; and the University of Granada trough the Plan Propio Program P9 Call-2013 contract and project UCE-PP2017. Andrés Bedoya has been supported by a grant for PhD studies in Colombia, COLCIENCIAS (Doctorado Nacional – 647) associated with the Physics Sciences program at the Universidad Nacional de Colombia, Sede Medellín and the Asociación Universitaria Iberoamericana de Postgrado (AUIP). Financial support for EARLINET was provided through the ACTRIS-2 Research Infrastructure Project EU H2O20 (Grant agreement no. 654109), particularly the TNA 3-SIR AHEAAARS. The authors gratefully acknowledge the FEDER program for the instrumentation used in this work. J. A. Bravo-Aranda has received funding from the Marie Sklodowska-Curie Action Cofund 2016 EU project – Athenea3i under grant agreement No 754446.

References

Bedoya-Velásquez, A. E., Navas-Guzmán, F., Granados-Muñoz, M. J., Titos, G., Román, R., Casquero-Vera, J. A., Ortiz-Amezcua, P., Benavent-Oltra, J. A., de Arruda Moreira, G., Montilla-Rosero, E., Hoyos, C. D., Artiñano, B., Coz, E., Olmo-Reyes, F. J., Alados-Arboledas, L., and Guerrero-Rascado, J. L.: Hygroscopic growth study in the framework of EARLINET during the SLOPE I campaign: synergy of remote sensing and in situ instrumentation, Atmos. Chem. Phys., 18, 7001-7017, https://doi.org/10.5194/acp-18-7001-2018, 2018.

Chen, J., Zhao, C.S., Ma, N., Yan, P.: Aerosol hygroscopicity parameter derived from the light scattering enhancement factor measurements in the North China Plain. Atmos. Chem. Phys. 14, 8105e8118, 2014.

Chen, J., Budisulistiorini, S. H., Miyakawa, T., Komazaki, Y., and Kuwata, M.: Secondary aerosol formation promotes water uptake by organic-rich wildfire haze particles in equatorial Asia, Atmos. Chem. Phys., 18, 7781-7798, https://doi.org/10.5194/acp-18-7781-2018, 2018.

Covert, D. S., Charlson, R. J., and Ahlquist, N. C.: A study of the relationship of chemical composition and humidity to light scattering by aerosols, J. Appl. Meteorol., 11, 968–976, 1972.

Crenn, V., Sciare, J., Croteau, P. L., Verlhac, S., Fröhlich, R., Belis, C. A., Aas, W., Äijälä, M., Alastuey, A., Artiñano, B., Baisnée, D., Bonnaire, N., Bressi, M., Canagaratna, M., Canonaco, F., Carbone, C., Cavalli, F., Coz, E., Cubison, M. J., Esser Gietl, J. K., Green, D. C., Gros, V., Heikkinen, L., Herrmann, H., Lunder, C., Minguillòn, M. C., Mocnik, G., O'Dowd, C. D., Ovadnevaite, J., Petit, J. E., Petralia, E., Poulain, L., Priestman, M., Riffault, V., Ripoll, A., Sarda-Estève, R., Slowik, J. G., Setyan, A., Wiedensohler, A., Baltensperger, U., Prévøt, A. S. H., Jayne, J. T., and Favez, O.: ACTRIS ACSM intercomparison – Part 1: Reproducibility of concentration and fragment results from 13 individual Quadrupole Aerosol Chemical Speciation Monitors (Q-ACSM) and consistency with co-located instruments, Atmos. Meas. Tech., 8, 5063–5087, 2015.

Dupont, J.-C., Haeffelin, M., Badosa, J., Elias, T., Favez, O., Petit, J.-E., Meleux, F., Sciare, J., Crenn, V., and Bonne, J.-L.: Role of the boundary layer dynamics effects on an extreme air pollution event in Paris, Atmos. Environ., 141, 571-579, doi: 10.1016/j.atmosenv.2016.06.061, 2016.

Feingold, G. and Morley, B.: Aerosol hygroscopic properties as measured by lidar and comparison with in situ measurements, J. Geophys. Res., 108, D11, https://doi.org/10.1029/2002JD002842, 2003.

Fernández, A. J., Apituley, A., Veselovskii, I., Suvorina, A., Henzing, J., Pujadas, M., and Artiñano., B.: Study of aerosol hygroscopic events over Cabauw experimental site for atmospheric research (CESAR) using the multi-wavelength Raman lidar Caeli, Atmos. Environ., 120, 484–498, 2015.

Fernández, J., Molero, F., Becerril-Valle, M., Coz, E., Salvador, P., Artíñano, B., Pujadas, M.: Application of remote sensing techniques to study aerosol water vapor uptake in a real atmosphere, Atmospheric Research, Volume 202, Pages 112-127, ISSN 0169-8095, https://doi.org/10.1016/j.atmosres.2017.11.020, 2018.

Ferrare, R. A., Melfi, S. H., Whiteman, D. N., Evans, K. D., and Leifer, R.: Raman lidar measurements of aerosol extinction and backscattering. 1. Methods and comparisons, J. Geophys. Res., 103, 19663–19672, 1998.

Freney, E., Zhang, Y., Croteau, P., Amodeo, T., Williams, L., Truong, F., Petit, J.-E., Sciare, J., Sarda-Estève, R., Bonnaire, N., Arumae, T., Aurela, M., Bougiatioti, E., Mihalopoulos, N., Coz, E., Artinano, B., Crenn, V., Elste, T., Heikkinen, L., Poulain, L., Wiedensohler, A., Herrmann, H., Priestman, M., Alastuey, A., Stavroulas, I., Tobler, A., Vasilescu, J., Zanca, N., Canagaratna, M., Carbone, C., Flentje, H., Green, D., Maasikmets, M., Marmureanu, L., Minguillon, M.-C., Prévôt, A. S. H., Gros, V., Jayne, J. T., and Favez, O.: The second ACTRIS inter-comparison (2016) for Aerosol Chemical Speciation Monitors

(ACSM): Calibration protocols and instrument performance evaluations, Aerosol Sci. Technol., Aerosol Science and Technology, DOI: 10.1080/02786826.2019.1608901, 2019.

Granados-Muñoz, M. J., Navas-Guzmán, F., Bravo-Aranda, J. A., Guerrero-Rascado, J. L., Lyamani, H., Valenzuela, A., Titos, G., Fernández-Gálvez, J., and Alados-Arboledas, L.: Hygroscopic growth of atmospheric aerosol particles based on active remote sensing and radiosounding measurements: selected cases in southeastern Spain, Atmos. Meas. Tech., 8, 705–718, https://doi.org/10.5194/amt-8-705-2015, 2015.

Haeffelin, M., Barthès, L., Bock, O., Boitel, C., Bony, S., Bouniol, D., Chepfer, H., Chiriaco, M., Cuesta, J., Delanoë, J., Drobinski, P., Dufresne, J.-L., Flamant, C., Grall, M., Hodzic, A., Hourdin, F., Lapouge, F., Lemaître, Y., Mathieu, A., Morille, Y., Naud, C., Noël, V., O'Hirok, W., Pelon, J., Pietras, C., Protat, A., Romand, B., Scialom, G., and Vautard, R.: SIRTA, a ground-based atmospheric observatory for cloud and aerosol research, Ann. Geophys., 23, 253–275, doi:10.5194/angeo-23-253-2005, 2005.

Haeffelin, M., Laffineur, Q., Bravo-Aranda, J.-A., Drouin, M.-A., Casquero-Vera, J.-A., Dupont, J.-C., and De Backer, H.: Radiation fog formation alerts using attenuated backscatter power from automatic lidars and ceilometers, Atmos. Meas. Tech., 9, 5347-5365, https://doi.org/10.5194/amt-9-5347-2016, 2016.

Hänel, G.: The Properties of Atmospheric Aerosol Particles as Functions of the Relative Humidity at Thermodynamic Equilibrium with the Surrounding Moist Air, in: Advances in Geophysics, edited by: Landsberg, H. E. and Mieghem, J. V., Elsevier, 73–188, 1976.

Jefferson, A., Hageman, D., Morrow, H., Mei, F., and Watson, T.: Seven years of aerosol scattering hygroscopic growth measurements from SGP: Factors influencing water uptake, J. Geophys. Res. Atmos., 122, doi:10.1002/2017JD026804, 2017.

Kamilli, K. A., Poulain, L., Held, A., Nowak, A., Birmili, W., and Wiedensohler, A.: Hygroscopic properties of the Paris urban aerosol in relation to its chemical composition, Atmos. Chem. Phys., 14, 737-749, https://doi.org/10.5194/acp-14-737-2014, 2014.

Kotchenruther, R. A., Hobbs, P. V., and Hegg, D. A.: Humidification factors for atmospheric aerosol off the mid-Atlantic coast of United States, J. Geophys. Res., 104(D2), 2239–2252, 1999.

Kotthaus, S., O'Connor, E., Münkel, C., Charlton-Perez, C., Haeffelin, M., Gabey, A. M., and Grimmond, C. S. B.: Recommendations for processing atmospheric attenuated backscatter profiles Atmos. Meas. Tech., 9, 5347–5365, 2016 from Vaisala CL31 ceilometers, Atmos. Meas. Tech., 9, 3769–3791, doi:10.5194/amt-9-3769-2016, 2016.

Lv M., Liu D., Li Z., Mao J., Sun Y., Wang Z., Wang Y. and Chenbo X.: hygroscopic growth of atmospheric aerosol particles based on lidar, radiosonde, and in situ measurements: case studies from the Xinzhou field campaign. Journal of quantitative spectroscopy & Raditive Transfer ,188 60-70, 2017.

Madonna, F., Amato, F., Vande Hey, J., and Pappalardo, G.: Ceilometer aerosol profiling versus Raman lidar in the frame of the INTERACT campaign of ACTRIS, Atmos. Meas. Tech., 8, 2207–2223, doi:10.5194/amt-8-2207-2015, 2015.

Navas-Guzmán, F., Fernández-Gálvez, J., Granados-Muñoz, M.J, Guerrero-Rascado, J.L., Bravo-Aranda, J.A., and Alados-Arboledas, L.: Tropospheric wáter vapor and relative humidiyty profiles from lidar and microwave radiometry. Atmos. Meas. Tech., 7, 1201-1211, 2014.

Pappalardo, G., Amodeo, A., Apituley, A., Comeron, A., Freudenthaler, V., Linné, H., Ansmann, A., Bösenberg, J., D'Amico, G., Mattis, I., Mona, L., Wandinger, U., Amiridis, V., Alados-Arboledas, L., Nicolae, D., and Wiegner, M.: EARLINET: towards an advanced sustainable European aerosol lidar network. Atmos. Meas. Tech., 7, 2389-2409, doi:10.5194/amt-7-2389-2014, 2014.

Petit, J.-E., Favez, O., Sciare, J., Canonaco, F., Croteau, P., Mo P., MoP., Mo, P., MoWorsnop, D., and Leoz-Garziandia, E.: Submicron aerosol source apportionment of wintertime pollution in Paris, France by double positive matrix factorization (PMF2) using an aerosol chemical speciation monitor (ACSM) and a multi-wavelength Aethalometer, Atmos. Chem. Phys., 14, 13773-13787, 10.5194/acp-14-13773-2014, 2014.

Petit, J.-E., Favez, O., Sciare, J., Crenn, V., Sarda-Estda-, R., Bonnaire, N., Mo, N., MoN.Dupont, J. C., Haeffelin, M., and Leoz-Garziandia, E.: Two years of near real-time chemical composition of submicron aerosols in the region of Paris using an Aerosol Chemical Speciation Monitor (ACSM) and a multi-wavelength Aethalometer, Atmos. Chem. Phys., 15, 2985-3005, 10.5194/acp-15-2985-2015, 2015.

Petit, J.-E., Amodeo, T., Meleux, F., Bessagnet, B., Menut, L., Grenier, D., Pellan, Y., Ockler, A., Rocq, B., Gros, V., Characterising an intense PM pollution episode in March 2015 in France from multi-site approach and near real time data: Climatology, variabilities, geographical origins and model evaluation. Atmos. Environ. 155, 68-84, 2017.

Pilinis, C. and Pandis, S. N.: Physical, Chemical and Optical Properties of Aerosols, in: The Handbook of Environmental Chemistry, edited by: Huntzinger, O., Springer Verlag, Heidelberg, Germany, 99–124, 1995.

Putaud, J.-P., Van Dingenen, R., Alastuey, A., Bauer, H., Birmili, W., Cyrys, J., Flentje, H., Fuzzi, S., Gehrig, R., Hansson, H. C., Harrison, R. M., Herrmann, H., Hitzenberger, R. , Huglin, C., ¨ Jones, A. M., Kasper-Giebl, A., Kiss, G., Kousa, A., Kuhlbusch, T. A. J., Loschau, G., Maenhaut, W., Molnar, A., Moreno, T., ¨ Pekkanen, J., Perrino, C., Pitz, M., Puxbaum, H., Querol, X., Rodriguez, S., Salma, I., Schwarz, J., Smolik, J., Schneider, J., Spindler, G., ten Brink, H., Tursic, J., Viana, M., Wiedensohler, A., and Raes, F.: A European aerosol phenomenology – 3: Physical and chemical characteristics of particulate matter from 60 rural, urban, and kerbside sites across Europe, Atmos. Env., 44, 1308–1320, 2010.

Randriamiarisoa, H., Chazette, P., Couvert, P., Sanak, J., and Mégie, G.: Relative humidity impact on aerosol parameters in a Paris suburban area, Atmos. Chem. Phys., 6, 1389-1407, https://doi.org/10.5194/acp-6-1389-2006, 2006.

Rosati, B., Wehrle, G., Gysel, M., Zieger, P., Baltensperger, U., and Weingartner, E.: The white-light humidified optical particle spectrometer (WHOPS) – a novel airborne system to characterize aerosol hygroscopicity, Atmos. Meas. Tech., 8, 921–939, https://doi.org/10.5194/amt-8-921-2015, 2015.

Rosati, B., Herrmann, E., Bucci, S., Fierli, F., Cairo, F., Gysel, M., Tillmann, R., Größ, J., Gobbi, G. P., Di Liberto, L., Di Donfrancesco, G., Wiedensohler, A., Weingartner, E., Virtanen, A., Mentel, T. F., and Baltensperger, U.: Studying the vertical aerosol extinction coefficient by comparing in situ airborne data and elastic backscatter lidar, Atmos. Chem. Phys., 16, 4539-4554, https://doi.org/10.5194/acp-16-4539-2016, 2016.

Sheridan, P.J., Jefferson, A., Ogren, J.A.: Spatial variability of submicrometer aerosol radiative properties over the Indian Ocean during INDOEX. J. Geophys. Res. 107 (D19), 8011, 2002.

Sorooshian, A., Hersey, S., Brechtel, F. J., Corless, A., Flagan, R. C., and Seinfeld, J. H.: Size-Resolved Aerosol Hygroscopic Growth Measurements: Differential Aerosol Sizing and Hygroscopicity Spectrometer Probe (DASH-SP), Aerosol. Sci. Tech., 42:6, 445-464, DOI: 10.1080/02786820802178506, 2008.

Swietlicki, E., Hansson, H. C., Hämeri, K., Svenningsson, B., Massling, A., Mcfiggans, G., Mcmurry, P. H., Petäjä, T., Tunved, P., Gysel, M., Topping, D., Weingartner, E., Baltensperger, U., Rissler, J., Wiedensohler, A., and Kulmala, M.: Hygroscopic properties of submicrometer atmospheric aerosol particles measured with H-TDMA instruments in various environments – a review, Tellus B, 6, 432–469, 2008.

Titos, G., Lyamani, H., Cazorla, A., Sorribas, M., Foyo-Moreno, I., Wiedensohler, A., Alados-Arboledas, L.: Study of the relative humidity dependence of aerosol light-scattering in southern Spain. Tellus B 66, 24536. http://dx.doi.org/10.3402/tellusb.v66.24536, 2014a.

Titos, G., Jefferson, A., Sheridan, P. J., Andrews, E., Lyamani, H., Alados-Arboledas, L., and Ogren, J. A.: Aerosol light-scattering enhancement due to water uptake during the TCAP campaign, Atmos. Chem. Phys., 14, 7031–7043, doi:10.5194/acp-14-7031-7043,2014b.

Titos, G., Cazorla, A., Zieger, P., Andrews, E., Lyamani, H., Granados- Muñoz, M. J., Olmo, F. J., and Alados-Arboledas, L.: Effect of hygroscopic growth on the aerosol light-scattering coefficient: A review of measurements, techniques and error sources, Atmos. Environ., 141, 494–507, 2016.

Veselovskii, I., Whiteman, D. N., Kolgotin, A., Andrews, E., and Korenskii, M.: Demonstration of aerosol property profiling by multi-wavelength lidar under varying relative humidity conditions, J. Atmos. Ocean. Tech., 26, 1543–1557, 2009.

Wiegner, M. and Geiß, A.: Aerosol profiling with the Jenoptik ceilometer CHM15kx, Atmos. Meas. Tech., 5, 1953–1964, doi:10.5194/amt-5-1953-2012, 2012.

Wiegner, M. and Gasteiger, J.: Correction of water vapor absorption for aerosol remote sensing with ceilometers, Atmos. Meas. Tech., 8, 3971–3984, doi:10.5194/amt-8-3971-2015, 2015.

Wiegner, M., Mattis, I., Pattantyús-Ábrahám, M., Bravo-Aranda, J. A., Poltera, Y., Haefele, A., Hervo, M., Görsdorf, U., Leinweber, R., Gasteiger, J., Haeffelin, M., Wagner, F., Cermak, J., Komínková, K., Brettle, M., Münkel, C., and Pönitz, K.: Aerosol backscatter profiles from ceilometers: validation of water vapor correction in the framework of CeiLinEx2015, Atmos. Meas. Tech. Discuss., https://doi.org/10.5194/amt-2018-307, in review, 2018.

Zhang, Q., Jimenez, J. L., Canagaratna, M. R., Allan, J. D., Coe, H., Ulbrich, I., Alfarra, M. R., Takami, A., Middlebrook, A. M., Sun, Y. L., Dzepina, K., Dunlea, E., Docherty, K., De-Carlo, P. F., Salcedo, D., Onasch, T., Jayne, J. T., Miyoshi, T., Shimono, A., Hatakeyama, S., Takegawa, N., Kondo, Y., Schneider, J., Drewnick, F., Borrmann, S., Weimer, S., Demerjian, K., Williams, P., Bower, K., Bahreini, R., Cottrell, L., Griffin, R. J., Rautiainen, J., Sun, J. Y., Zhang, Y. M., and Worsnop, D. R.: Ubiquity and dominance of oxygenated species in organic aerosols in anthropogenically-influenced Northern Hemisphere midlatitudes, Geophys. Res. Lett., 34, L13801, doi:10.1029/2007GL029979, 2007.

Zhang, L., Sun, J.Y., Shen, X.J., Zhang, Y.M., Che, H.C., Ma, Q.L., Zhang, Y.W., Zhang, X.Y., Ogren, J.A.: Observations of relative humidity effects on aerosol light scattering in the Yangtze River Delta of China. Atmos. Chem. Phys.15, 8439e8454. http://dx.doi.org/10.5194/acpd-15-2853-2015, 2015.

Zieger, P., Weingartner, E., Henzing, J., Moerman, M., de Leeuw, G., Mikkilä, J., Ehn, M., Petäjä, T., Clémer, K., van Roozendael, M., Yilmaz, S., Frieß, U., Irie, H., Wagner, T., Shaiganfar, R., Beirle, S., Apituley, A.,Wilson, K., and Baltensperger, U.: Comparison of ambient aerosol extinction coefficients obtained from in situ, MAX-DOAS and LIDAR measurements at Cabauw, Atmos. Chem. Phys., 11, 2603–2624, https://doi.org/10.5194/acp- 11-2603-2011, 2011.

Zieger, P., Fierz-Schmidhauser, R., Poulain, L., Müller, T., Birmili, W., Spindler, G., Wiedensohler, A., Baltensperger, U., Weingartner, E.: Influence of water uptake on the aerosol particle light scattering coefficients of the Central European aerosol. Tellus B 66, 22716. http://dx.doi.org/10.3402/tellusb.v66.22716, 2014.

Table 1: Enhancement factor (f_β (RH=85 %)) at RH_{ref} of the case and extrapolated at RH_{ref}=40 %, γ, wind speed, variability of wind speed and wind direction and the index of variability between Δf_{PM1} and $\Delta f_\beta(RH)$. These variables are used to perform the analysis of the aerosol hygroscopic cases.

	RH_{ref} [%]	$\beta_{ref}[m^{-1}Sr^{-1}]$	f_β(RH=85)	f_β(RH=85/40)	γ	W_s [m/s]	ΔW_s [%]	ΔW_d [%]	RI
Case 1: 2012/07/29	52.9	6.2E-7	1.8±0.2	2.3 ±0.2	0.6±0.6	1	14.2	3.6 (W)	0.7
Case 2: 2012/09/02	49.6	6.6E-7	2.1±0.2	2.6±0.2	0.7±0.4	2.5	20.7	23.0 (NW)	0.7
Case 3: 2013/06/25	57.3	9.1E-7	1.7±0.2	2.0±0.2	0.5±0.4	2.5	24.5	33.9 (NW)	0.6
Case 4: 2014/07/28	53.7	5.1E-7	2.2±0.2	2.6±0.2	0.7±0.7	5	15.4	2.7 (W)	0.7
Case 5: 2014/08/17	56.7	4.1E-7	1.6±0.1	2.0±0.1	0.5±0.2	5.5	20.4	2.4 (SW)	0.8
Case 6: 2015/05/21	55.1	6.7E-7	2.4±0.2	3.0±0.2	0.7±0.4	2.5	18.5	4.4 (W)	0.5

Case 7: 2016/04/15	51.6	8.6E-7	2.3±0.3	3.0±0.3	0.8±0.3	6	10.9	1.7 (SW)	0.6
Case 8: 2016/05/17	47.1	7.2E-7	2.5±0.3	3.3±0.3	0.9±0.6	3	20.7	6.4 (W)	0.6

Table 2: Linear fits of the extrapolated f_β (85/40) versus OMF and IMF for the eight cases found. The values of the adjustments between γ and OMF/IMF are also reported. Finally, regarding the amount of IA (Fo), Fo is defined by (a) $Fo = OA/(OA + SO_4^{2-})$, (b) Fo=$OA/(OA + NO_3^-)$ and (c) Fo=$OA/(OA + SO_4^{2-} + NO_3^-)$ and linearized versus γ.

	SLOPE	**INTERCEPT**	**R^2**
$\boldsymbol{f_\beta\ (RH = 85/40)}$ **vs OMF**	-4.81 ± 0.04	5.3± 0.1	0.60
$\boldsymbol{f_\beta\ (RH = 85/40)\ vs}$ **IMF**	3.8 ± 0.1	1.1 ± 0.1	0.40
$\boldsymbol{\gamma}$ **vs OMF**	-1.5 ± 0.1	1.5 ± 0.1	0.67
$\boldsymbol{\gamma}$ **vs IMF**	1.2 ± 0.1	0.2 ± 0.1	0.42
$\boldsymbol{\gamma}$ **vs** $\boldsymbol{Fo}$ **=**$\boldsymbol{(OA/(OA + SO_4^{2-}))}$	-0.7 ± 0.2	1.2 ± 0.2	0.18
$\boldsymbol{\gamma}$ **vs** $\boldsymbol{Fo}$ **=**$\boldsymbol{(OA/(OA + NO_3^-))}$	-1.3 ± 0.1	1.8 ± 0.1	0.32
$\boldsymbol{\gamma}$ **vs** $\boldsymbol{Fo}$ **=** $(\boldsymbol{OA/(OA + SO_4^{2-} + NO_3^-)})$	-1.2 ± 0.2	1.4 ± 0.1	0.40

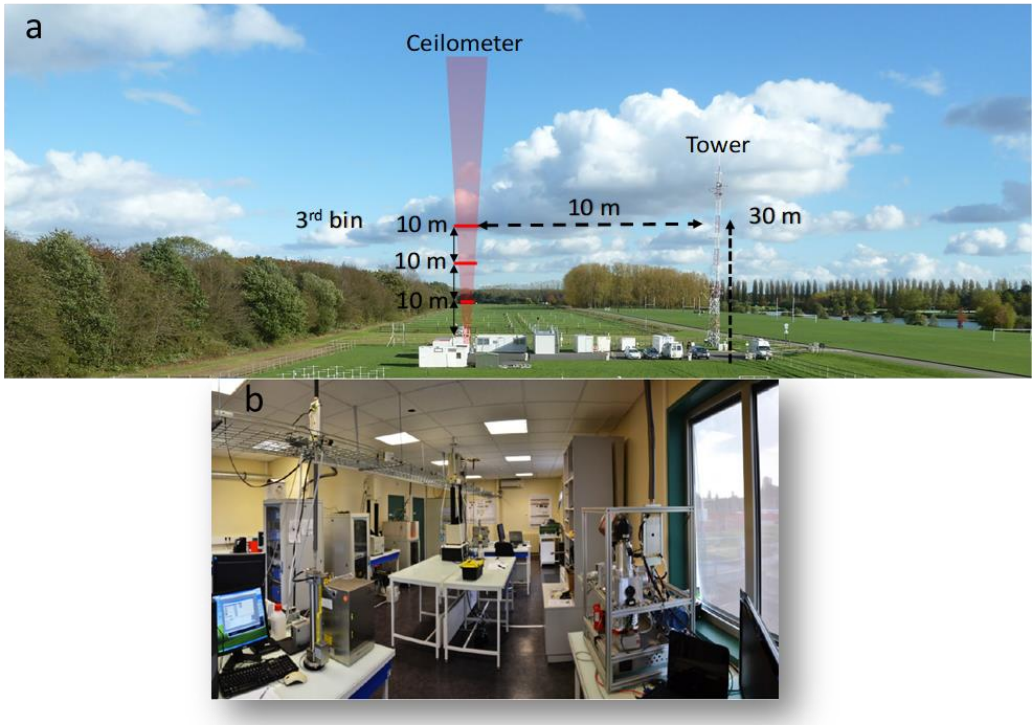

Figure 1: (a) Experimental setup (not 1:1 scale) for studying hygroscopic growth using the automatic instrumentation (ceilometer and hygrometer) and (b) in situ monitoring station at the ACTRIS SIRTA observatory.

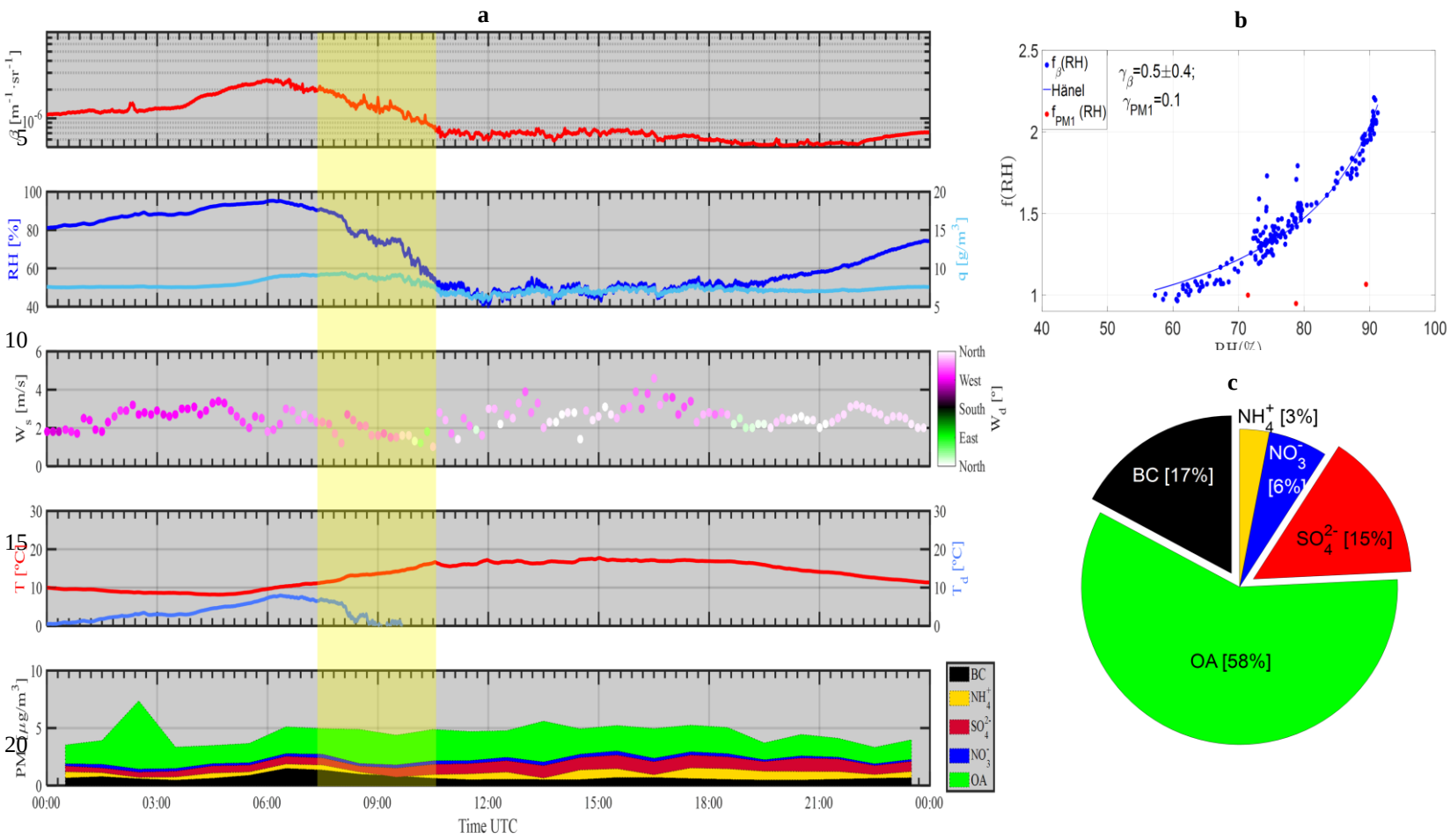

Figure 2: Case 3 on 25 June 2013: (a) time series of β (relative humidity, RH; absolute humidity, q; wind speed, Ws; wind direction, Wd; temperature, T; dew point temperature, Td) and PM_1 chemical species concentration according to the legend; (b) PM_1-related $f_{PM1}(RH)$ and β-related $f_\beta(RH)$; and (c) pie chart of the chemical composition. (b) and (c) are measured for the hygroscopic event time-window. The highlighted region in yellow (from 07:17 to 10:17 UTC) represents the time window where the aerosol hygroscopic growth is evaluated.

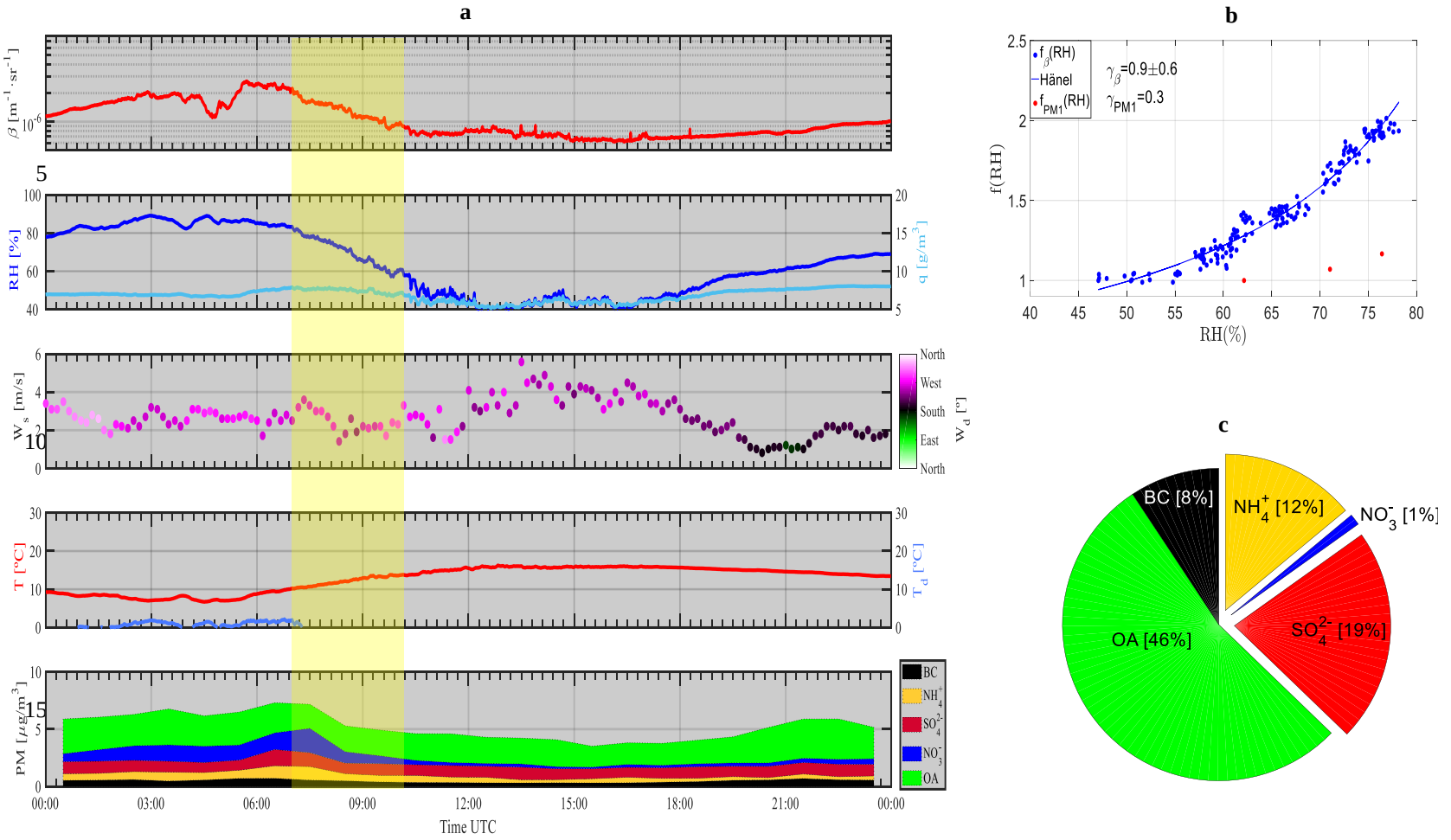

Figure 3: As noted in Figure 2 but using case 8 on 17 May 2016 with the highlighted region from 07:40 to 10:40 UTC.

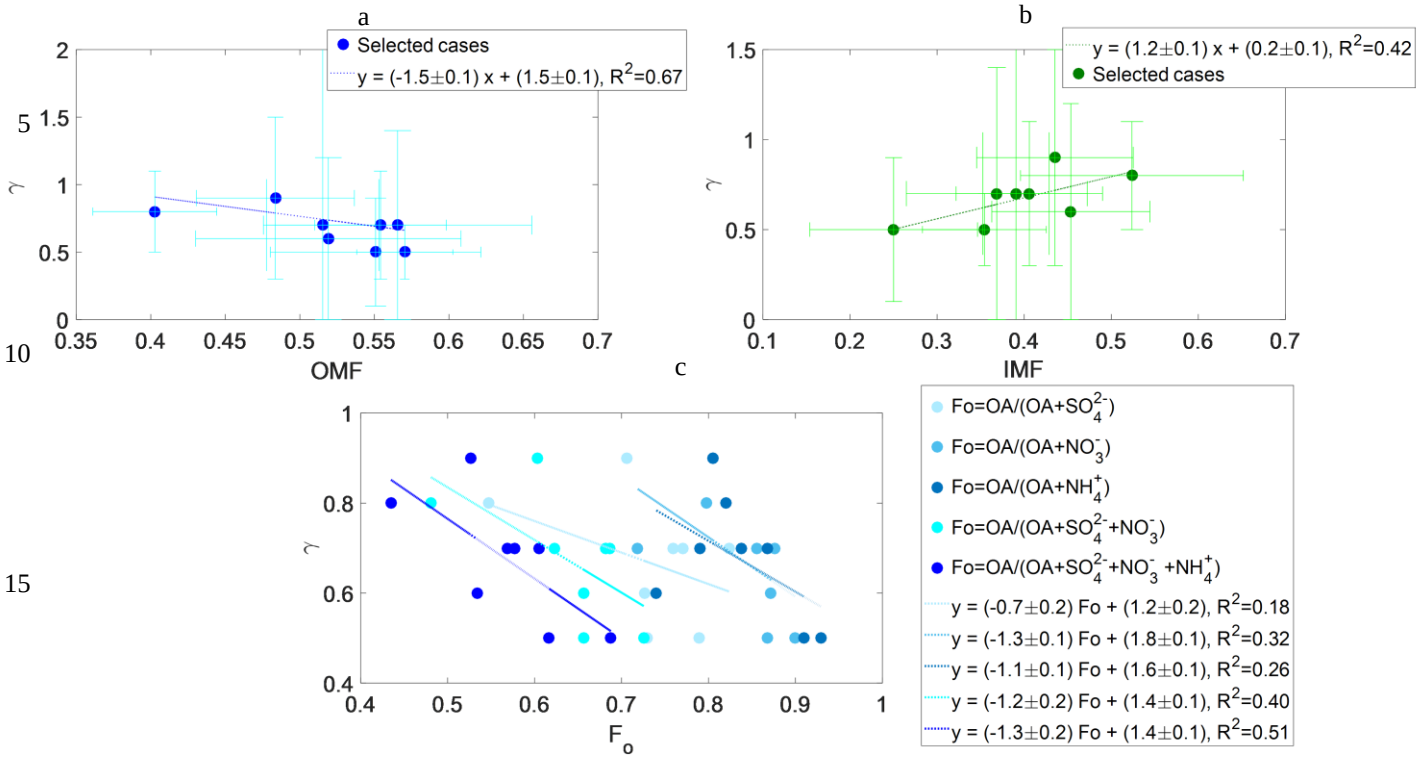

Figure 4: Mass fraction and γ parameter correlation for the eight hygroscopic growth cases. (a) The OMF against γ is noted in blue dots with error bars, and the dashed line is the linear fit; (b) the IMF and γ correlation is noted in green dots with the respective error bars of the gamma and the OMF/IMF uncertainties, and the dashed line represents the linear fit; and (c) the correlations of the relative amount of OA and IA (Fo) versus γ. Fo is defined according to the legend.